CTP synthase is essential for early endosperm development by regulating nuclei spacing

Jinmi Yoon[1,2,†], Lae-Hyeon Cho[1,2,†] (iD), Sung-Ryul Kim[3,†], Win Tun[1], Xin Peng[1,4], Richa Pasriga[1], Sunok Moon[1], Woo-Jong Hong[1], Hyeonso Ji[5], Ki-Hong Jung[1] (iD), Jong-Seong Jeon[1] (iD) and Gynheung An[1,*] (iD)

[1]*Crop Biotech Institute and Graduate School of Biotechnology, Kyung Hee University, Yongin, Republic of Korea*

[2]*Department of Plant Bioscience, College of Natural Resources and Life Science, Pusan National University, Miryang, Republic of Korea*

[3]*Gene Identification and Validation Group, Genetic Design and Validation Unit, International Rice Research Institute (IRRI), Metro Manila, Philippines*

[4]*Institution of Genomics and Bioinformatics, South China Agricultural University, Guangzhou, China*

[5]*National Institute of Agricultural Sciences, Rural Development Administration, Jeonju, Republic of Korea*

Summary

Cereal grain endosperms are an important source of human nutrition. Nuclear division in early endosperm development plays a major role in determining seed size; however, this development is not well understood. We identified the rice mutant *endospermless 2* (*enl2*), which shows defects in the early stages of endosperm development. These phenotypes arise from mutations in *OsCTPS1* that encodes a cytidine triphosphate synthase (CTPS). Both wild-type and mutant endosperms were normal at 8 h after pollination (HAP). In contrast, at 24 HAP, *enl2* endosperm had approximately 10–16 clumped nuclei while wild-type nuclei had increased in number and migrated to the endosperm periphery. Staining of microtubules in endosperm at 24 HAP revealed that wild-type nuclei were evenly distributed by microtubules while the *enl2-2* nuclei were tightly packed due to their reduction in microtubule association. In addition, OsCTPS1 interacts with tubulins; thus, these observations suggest that OsCTPS1 may be involved in microtubule formation. OsCTPS1 transiently formed macromolecular structures in the endosperm during early developmental stages, further supporting the idea that OsCTPS1 may function as a structural component during endosperm development. Finally, overexpression of *OsCTPS1* increased seed weight by promoting endosperm nuclear division, suggesting that this trait could be used to increase grain yield.

Introduction

The endosperm is a major component of cereal grains that stores starch, proteins and several other types of nutrients required for seed germination and early growth (Lopes and Larkins, 1993). One of the discriminating features of endosperm development is that fertilized central cells undergo rapid nuclear division without cell wall formation during the early developmental stages (syncytium stages), resulting in the formation of a multinucleate cell (Olsen, 2004). The numbers of nuclei in endosperm syncytium are greater in cereals than in the model plant *Arabidopsis thaliana*, in which the syncytial endosperm carries approximately 200 nuclei (Bennett *et al.*, 1975). In contrast, during the first 1–2 days after pollination (DAP), rice endosperms produce 4,000–8,000 nuclei without accompanying cell division, which then migrate towards the periphery of the chalazal region of the embryo sac. Next, at 3–4 DAP, the syncytial endosperm is cellularized and cell walls are formed (Sabelli and Larkins, 2009). Endosperm cells then undergo rapid mitotic division from 4 to 10 DAP, endoreduplication from 8 to 10 DAP and programmed cell death from 14 to 20 DAP (Olsen, 2004).

Although several genes associated with cereal endosperm storage have been investigated, only a few genes affecting early endosperm development have been identified in rice (Kurata *et al.*, 2005; Zhou *et al.*, 2013). Rice plants with mutations in the gene *LEAF AND FLOWER-related* (*OsLFR*), which encodes an

interaction partner of SWITCH/SUCROSE NON-FERMENTABLE (SWI/SNF) in the ATP-dependent chromatin-remodelling complex, display abnormal endosperm development (Qi *et al.*, 2020). While the number of syncytial nuclei in *oslfr-1* and wild-type (WT) endosperm is similar at 24 hours after pollination (HAP), at 32 HAP and beyond, the number of free nuclei at the periphery of *oslfr-1* endosperm is much lower than in WT endosperm, suggesting that this gene functions in syncytial nuclei formation.

Regulatory genes affecting endosperm cellularization have also been identified. Suppression of *CycB1;1* expression creates an aberrant endosperm phenotype beginning from 2 DAP (Guo *et al.*, 2010). Although the *CycB1;1*-knock-down plants show normal distribution of endosperm nuclei to the sac periphery, cell walls fail to properly form, suggesting that *CycB1;1* is involved in cellularization. In addition, mutants defective in *MADS78* or *MADS79* exhibit precocious endosperm cellularization and the *mads78 mads79* double mutant is sterile (Paul *et al.*, 2020). Overexpression of *MADS78* and *MADS79* results in delayed endosperm cellularization, indicating that these transcription factors inhibit endosperm cellularization. Both MADS78 and MADS79 interact with MADS89, which enhances their nuclear localization, suggesting MADS89 is also involved in endosperm development (Paul *et al.*, 2020).

Genes involved in the later stages of endosperm development have also been identified. The endosperm of the rice mutant *endospermless* (*enl1*) is normal at 3 DAP but degenerates by later

stages, resulting in the production of a large embryo (Hong *et al.*, 1996). This mutant also develops enlarged nuclei due to a malfunction in mitotic chromosomal segregation in the syncytial endosperm. These phenotypes were later found to arise from a defect in an SNF2 family chromatin-remodelling helicase that is orthologous to human Plk1-interacting checkpoint helicase (Hara *et al.*, 2015). The transgenic plants with reduced expression of *NF-Y* carry a reduced number of endosperm cells, suggesting that this gene functions during mitosis as part of endosperm development (Sun *et al.*, 2014). Finally, endosperm mutants with defects in *OsCCS52A* display abnormalities during endoreduplication, reducing the amount of endosperm produced (Su'udi *et al.*, 2012).

Enlarged embryos have been observed for several endosperm mutants and appear to be associated with a lack of endosperm (Guo *et al.*, 2010; Hara *et al.*, 2015; Nagasawa *et al.*, 2013; Su'udi *et al.*, 2012; Sun *et al.*, 2014; Yang *et al.*, 2013). More specifically, endosperm-specific suppression of cell cycle inhibition creates endosperm defects and increased embryo size (Guo *et al.*, 2010). In addition, interactions between the embryo and endosperm at interface tissues appear to play critical roles in controlling relative embryo size (Nagasawa *et al.*, 2013).

Certain molecules form non-membrane-bound macromolecular structures that play important cellular roles, including histone locus bodies (Liu *et al.*, 2006), cytoplasmic processing bodies (Sheth and Parker, 2006), uridine-rich small nuclear ribonucleoprotein bodies (Liu and Gall, 2007) and purinosomes (An *et al.*, 2008). In addition, cytidine triphosphate synthase (CTPS) also appears to form macromolecular structures based on work in the bacterial species *Caulobacter crescentus* and *Escherichia coli* (Ingerson-Mahar *et al.*, 2010), *Drosophila* (Liu, 2010), budding yeast (*Saccharomyces cerevisiae*) (Noree *et al.*, 2010) and human tissue (Carcamo *et al.*, 2011; Chen *et al.*, 2011). In addition, inosine monophosphate dehydrogenase, which catalyses the rate-limiting reaction of *de novo* GTP biosynthesis, also forms macromolecular structures (Carcamo *et al.*, 2011).

In this study, we identified rice endosperm mutants containing alterations in rice *CTP synthase 1* (*OsCTPS1*). These mutants stopped the endosperm nuclei production at 24 HAP, with mutant nuclei remaining clustered and lacking sufficient radial microtubule systems (RMSs) between nuclei. In addition, mutant nuclei failed to migrate to the endosperm periphery, with these defects suggesting that OsCTPS1 is involved in microtubule formation. This hypothesis is further supported by evidence that OsCTPS1 interacts with tubulins. In addition, OsCTPS1 transiently forms macromolecular structures in syncytium endosperm.

Results

Identification of a mutant defective in endosperm development

We identified an individual from a *japonica* rice cultivar with defect in seed development. In this line, about 1/4 of seeds were abnormal and some germinated precociously (Figure 1a). Progeny exhibited entirely defective seeds, which indicated that the seed defects were due to a recessive mutation that was stably inherited. The ventral side of each seed was severely shrunken compared to the dorsal side (Figure 1b,c), and longitudinal sections of the developing seeds at 10 DAP showed that mutant seeds contained altered endosperm. In addition, the embryos of the mutant seeds were much bigger than those of WT seeds (Figure 1d). We thus named the mutant *endospermless2-1* (*enl2-*

1). Most mutant seeds germinated; however, their initial growth was slower than that of segregated WT seedlings. In addition, root development was significantly reduced in *enl2-1* mutants, as mutant primary roots were 41% shorter than those of WT controls at 10 days after germination (DAG) (Figure 1e,f). To examine whether the *enl2-1* mutants had decreased meristem activity, 7 DAG seedling roots were incubated with ethynyl deoxyuridine (EdU), which is incorporated into DNA during active DNA synthesis in S-phase cells. EdU visualization showed that *enl2-1* had a smaller root apical meristem than WT plants due to a decreased number of meristem cells (Figure 1g,h). However, the growth of *enl2-1* ultimately recovered and *enl2-1* plants flowered at the same time as their WT siblings.

Map-based cloning of *enl2-1*

In order to identify the gene responsible for *enl2-1* mutant phenotypes, we crossed the *enl2-1* mutant line with the *indica* type rice cultivar Milyang 23. Bulked segregant analysis was conducted with 77 simple sequence repeat (SSR) markers distributed over 12 chromosomes using segregating F_2 seeds (Ji *et al.*, 2006), with R1M30 on chromosome 1 being the closest marker to the phenotype-linked region (Figure 2a). To validate the identity of this phenotype-linked marker, 704 individual F_2 plants derived from normal and mutant seeds were genotyped with six InDel markers surrounding R1M30. Of the 251 resulting mutants, 228 (90.84%) possessed a homozygous *japonica* marker at R1M30 while 12 out of 453 normal seed-derived plants (2.65%) had the *japonica* marker at RM130, indicating that the *enl2-1* phenotypes are tightly linked to R1M30. Initial mapping indicated that the *enl2-1* mutations were present in a 1.45-Mb region between RM9 and R1M30 (Figure 2a). Genotyping of 1086 seeds (568 normal and 518 mutant) by the border markers RM9 and R1M30 identified 43 recombinants. Mapping of these recombinants narrowed the position of the mutant locus to a ~ 43-kb region between the S9697 and CBI12 markers that contains five annotated genes: *Os01g42970* (zinc finger domain protein), *Os01g42980* (ribosomal protein L22), *Os01g42990* (pentatricopeptide repeat domain protein), *Os01g43010* (transposon protein) and *Os01g43020* (CTP synthase) (Figure 2a).

Among these annotated genes, the coding regions of all genes except *Os01g43010* were sequenced from parental *japonica* and *enl2-1* mutant plants. Sequence analysis revealed a single nucleotide substitution from A to T in the third exon of *Os01g43020*, causing a change of Asn (N) to Ile (I) at 86th amino acid in a conserved CTP synthase domain (Figure 2b,c). No other alterations of the sequence were found in the four genes, indicating that the altered phenotypes of *enl2-1* were caused by this point mutation in *Os01g43020*. Since this locus encodes a protein that is highly homologous to CTP synthase and contains both conserved CTP synthase and glutamine amide transfer domains (Choi and Carman, 2007) (Figure 2c), we re-named *Os01g43020* as *Oryza sativa CTP synthase 1* (*OsCTPS1*). CTP synthase catalyses the ATP-dependent transfer of the amide nitrogen of glutamine to the C-4 position of UTP to generate CTP, which is the rate-limiting final step in *de novo* pyrimidine-nucleotide biosynthesis (Figure 2d) (Choi and Carman, 2007). Active CTP synthase is a tetrameric enzyme composed of a dimer of dimers, and its formation is favoured by the presence of the substrate nucleotides ATP and UTP (Figure 2e) (Iben et al., 2011). To determine whether *enl2-1* exhibits altered homodimerization, the homodimerization of OsCTPS1 and OsCTPS1-N86I (the OsCTPS1 form found in *enl2-1*) was examined using a co-
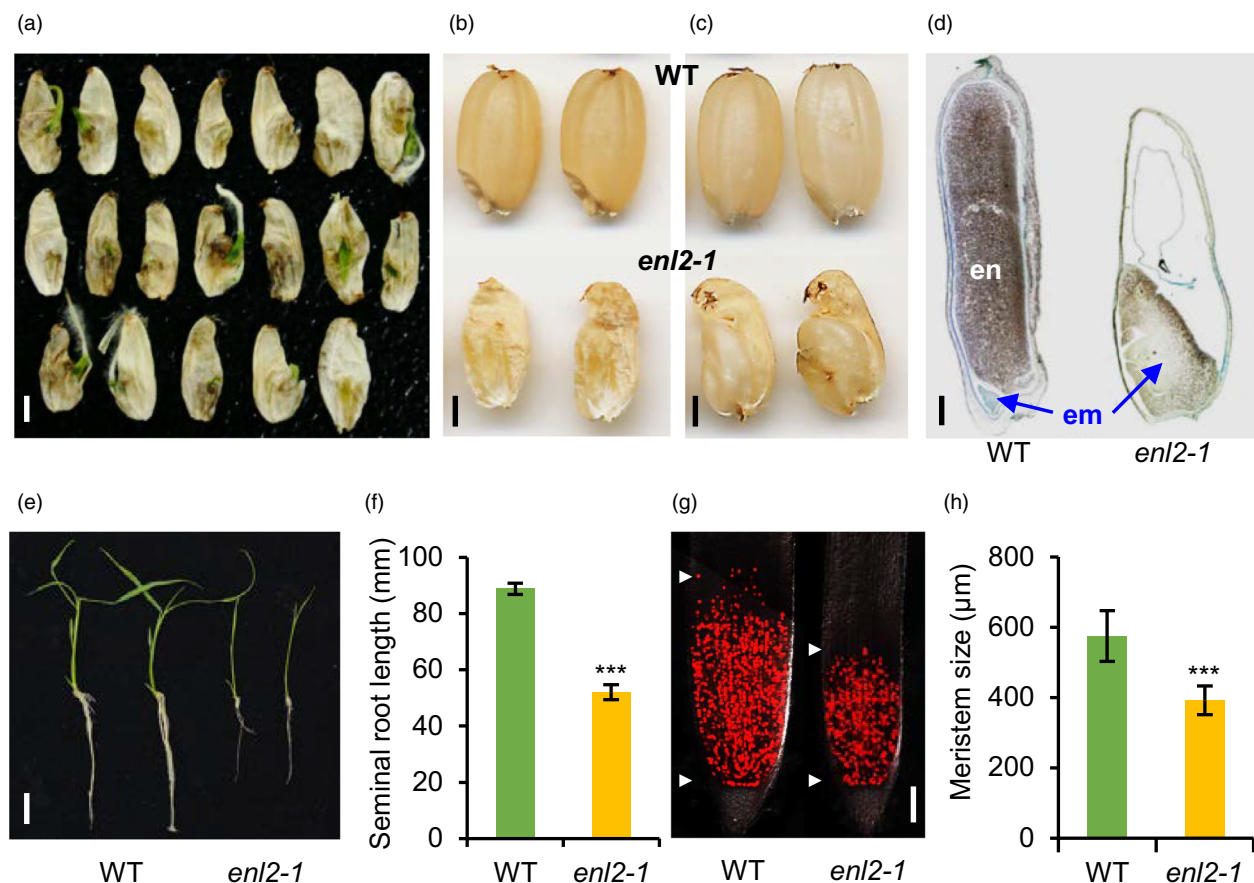
FIGURE 1 *enl2-1* phenotypes. (a) Phenotype of *enl2-1* seeds derived from the PFG_1C-15623 line. Scale bar, 1 mm. (b) The ventral side of *enl2-1* seeds. Scale bar, 1 mm. (c) The dorsal side of *enl2-1* seeds. Scale bar, 1 mm. (d) Longitudinal sections of WT and *enl2-1* seeds at 10 DAP. en, endosperm; em, embryo. Scale bar, 500 μm. (e) WT and *enl2-1* seedlings at 10 DAG. Scale bar, 2 cm. (f) Length of WT and *enl2-1* primary roots. Error bars show standard deviation $n = 6$. Statistical significance is indicated by *** ($P < 0.001$). (g) S-phase cells of WT and *enl2-1* primary roots at 7 DAG. Scale bar, 100 μm. (h) Average length of root meristematic regions. Error bars show standard deviation $n = 6$. Statistical significance is indicated by *** ($P < 0.001$). [Colour figure can be viewed at wileyonlinelibrary.com]

immunoprecipitation (Co-IP) assay (Figure 2f). OsCTPS1-N86I appeared to dimerize at similar levels as OsCTPS1 (Figure 2f). Analysis of enzyme activity showed that OsCTPS1-N86I had significantly reduced CTP synthase activity compared to OsCTPS1 (Figure 2g), revealing that the amino acid substitution N86I in the *enl2-1* mutant largely affects the enzyme activity of OsCTPS1, leading to a lack of endosperm.

Expression patterns of *OsCTPS1*

Six putative CTP synthase genes were found in the rice genome, which we named *OsCTPS1* (*Os01g43020*), *OsCTPS2* (*Os01g46570*), *OsCTPS3* (*Os05g49460*), *OsCTPS4* (*Os05g49520*), *OsCTPS5* (*Os05g49770*) and *OsCTPS6* (*Os12g36950*). Five *OsCTPS1-5* are clustered to monocot CTPS genes, while one *OsCTPS6* is closely related to dicot CTPS genes (Figure S1 and S2). Expression data found in public domains indicated that all six genes are ubiquitously expressed (Figure S3). We measured the expression levels of all six CTPS genes in developing seeds at 1 DAP, when *enl2-1* defects begin to appear, and saw that *OsCTPS1* was the most highly expressed CTPS family member (Figure 3a). The *OsCTPS1* expression pattern was then determined to evaluate whether the mutant phenotypes were caused by tissue specific in *OsCTPS1* expression. Quantitative RT-PCR analyses showed that *OsCTPS1* was expressed

ubiquitously in all of the samples and in developmental stages ranging from seedlings to mature plants (Figure 3b). However, *OsCTPS1* expression levels in both shoot apical meristems (SAMs) and panicles were approximately twofold higher than in leaves and internodes, although it is uncertain whether this difference is large enough to explain *enl2-1* mutant phenotypes.

To examine cellular level *OsCTPS1* expression, we generated transgenic rice plants expressing the *GUS* reporter gene under the control of the *OsCTPS1* promoter. The *GUS* expression was universally detected in all the organs examined (Figure 3c–h), with preferential expression in the stele and quiescent centre (QC) regions of roots (Figure 3d). Reporter expression levels were also higher in the SAM (Figure 3e) as well as the anthers and veins of developing spikes (Figure 3g,h). These results suggest that *OsCTPS1* expression is higher in dividing cells. In developing seeds, the *GUS* reporter was expressed throughout the embryo sac, with stronger staining observed in the endosperm and embryo (Figure 3i–l). Cross sections of developing seeds at 2 DAP showed that the reporter was uniformly expressed in the endosperm and nucellus, as well as pericarp cells (Figure 3l). These observations indicate that the mutant phenotypes were not likely caused by tissue specificity of *OsCTPS1* expression.
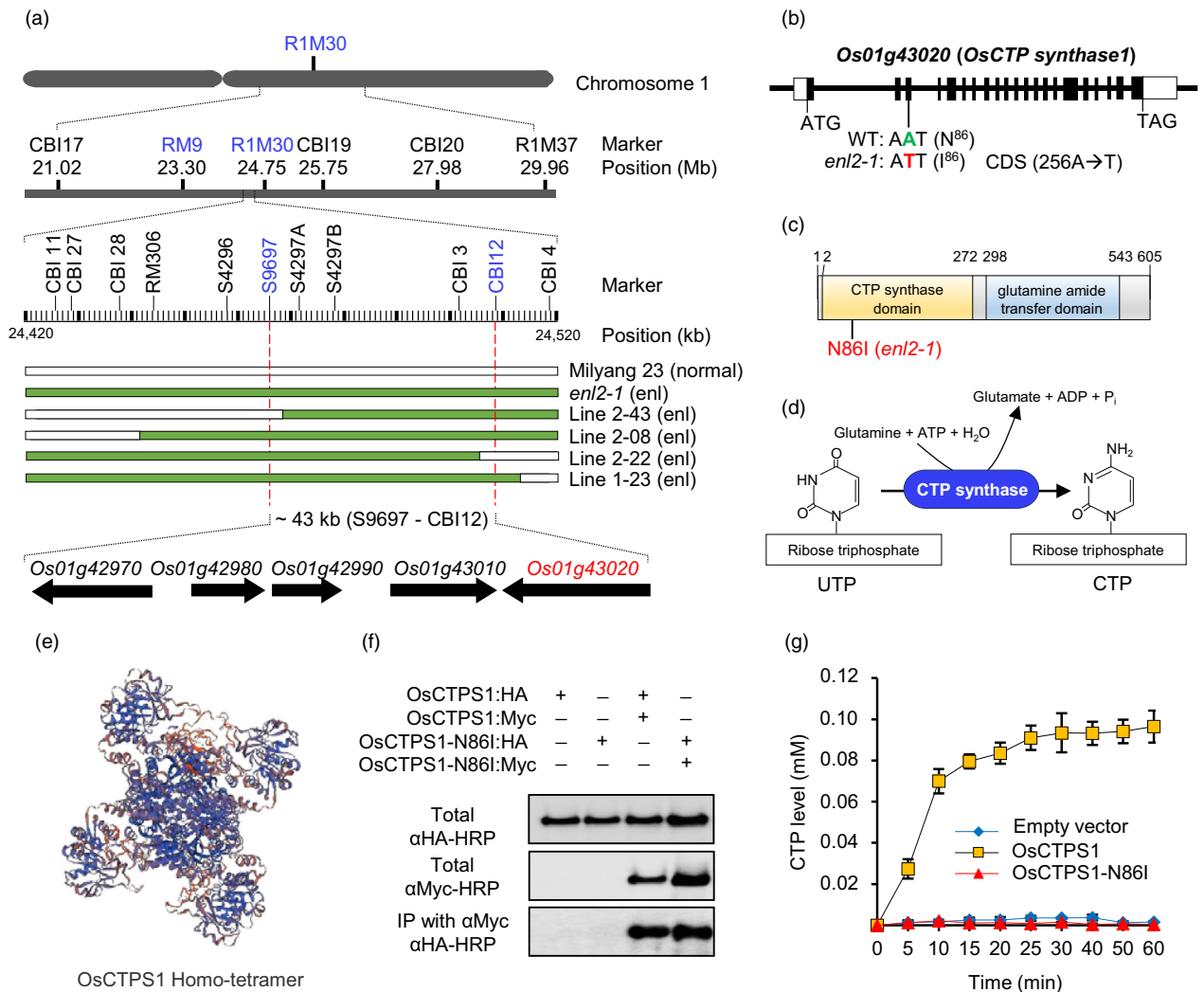
FIGURE 2 Map-based cloning of *enl2-1*. (a) The *enl2-1* locus is present within a 43-kb region that contains five annotated genes. Phenotype-linked markers are highlighted in blue. White bars indicate chromosomes from Milyang 23 while green bars indicate chromosomes from the *enl2-1* mutant. Phenotypes are noted in parenthesis. (b) The genomic structure of *Os01g43020* containing 20 introns and 21 exons. The nucleotide substitution in *enl2-1* (A to T) is indicated with colours. Closed and open boxes represent exons and UTRs, respectively. Lines between boxes are introns. The start and stop codons of *OsCTP synthase 1* are indicated. (c) The CTP synthase domain structure encoded by *Os01g43020*. The approximate positions of the CTP synthase domain and the glutamine amide transfer domain are noted. A single nucleotide mutation (A to T substitution) in *enl2-1* causes an asparagine-to-isoleucine conversion at amino acid position 86 (N86I). (d) The enzymatic reaction catalysed by CTP synthase. (e) The protein structures in the OsCTPS1 homotetramer as predicted by SWISS-MODEL. (f) Homodimerization of OsCTPS1 and OsCTPS1-N86I. OsCTPS1 and OsCTPS1-N86I were tagged with HA or Myc tags and then co-expressed in Oc cell protoplasts. Total protein extracts were immunoprecipitated using anti-Myc antibodies and interactions detected using anti-HA antibody following SDS-PAGE. (g) Enzymatic activity of OsCTPS1 and OsCTPS1-N81I. Purified wild-type OsCTPS1 and mutant OsCTPS1-N86I proteins were incubated at 37°C for the indicated amounts of time in the reaction mixture described in the Materials and Methods section. The empty pET28a (+) vector was used as a negative control. Error bars represent standard deviation $n = 3$. Data obtained from three independent biological replicates.

Generation and characterization of additional *OsCTPS1* alleles

To confirm that the phenotypes observed in the *enl2-1* mutant were indeed due to a defect in OsCTPS1 activity, we generated additional alleles of the gene using CRISPR/Cas9. The sgRNA target site was selected in the second exon to generate premature stop codons, thereby resulting in null alleles. Sequencing of several plants independently transformed with the CRISPR/Cas9 vector showed that two different deletions occurred at or near the target site in four plants (lines #1, #2, #3 and #4). We

also selected one plant (Line #5) that showed no alterations in the sequence as a WT control (Figure S4a).

All five transgenic plants grew normally throughout their entire lifetimes. However, all of the seeds from lines #1–4 containing *OsCTPS1* deletions were abnormal, whereas the WT control plant (Line #5) produced normal seeds (Figure S4b). The first four lines appeared to be biallelic at the primary transgenic stage due to two different deletions in each plant, and all of the seeds from each plant were abnormal (Figure S4 and Figure S5). We selected lines #1 (*enl2-2*) and #4 (*enl2-3*) for further analyses. While seeds from the *enl2-2* mutant germinated normally, the seedlings of gene-
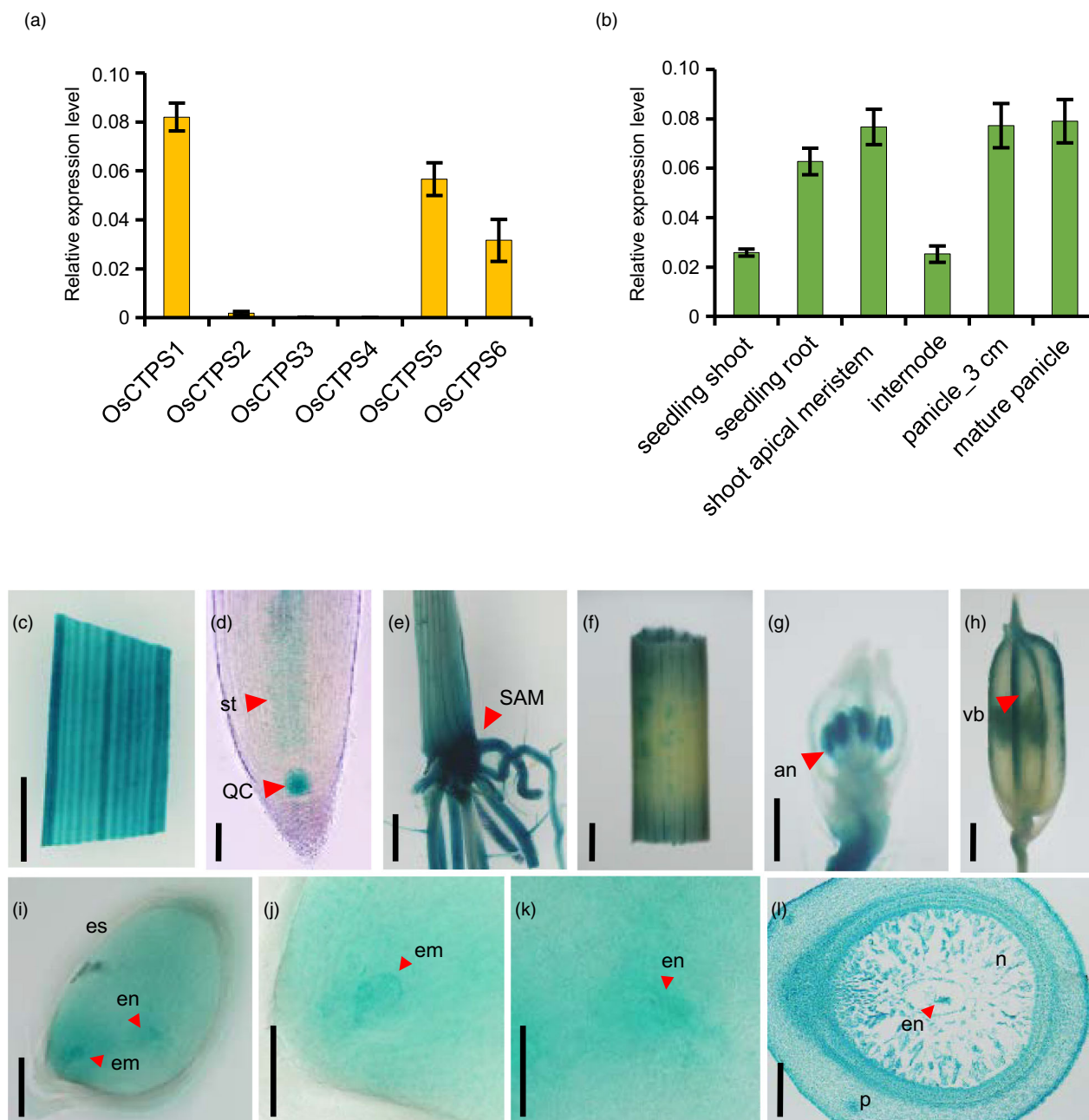
(a)

(b)

FIGURE 3 Expression patterns of *OsCTPS* genes. (a) Quantitative RT-PCR analyses of expression levels of six *OsCTPS* genes in developing seeds at 1 DAP. Error bars indicate standard deviation $n = 4$. (b) Quantitative RT-PCR analyses of expression levels of *OsCTPS1* in various organs. Error bars represent standard deviation $n = 4$. (c-l) Representative GUS expression patterns in a seedling leaf (c), seedling root (d), shoot apical meristem (e), internode (f), spikelet in 3-cm panicle (g), mature spikelet (h), embryo sac from a developing seed at 1 DAP (i-k) and in a cross-sectional image of a developing seed at 2 DAP (l). Scale bars, 2 mm (c), (e), (f), (h); 1 mm (g); 100 μm (d, i, l); 50 μm (j, k). st, stele; QC, quiescent centre; SAM, shoot apical meristem; an, anther; vb, vascular bundle; es, embryo sac; en, endosperm; em, embryo; n, nucellus; p, pericarp. Red arrows indicate GUS signal.

edited mutants grew slower than the WT control plants (Line #5) (Figure S6). However, growth was recovered at later developmental stages and headed at a similar time to WT (Figure S5a).

WT and *enl2-2* seeds were harvested at different developmental stages and compared. No significant difference was observed at 2 DAP; however, the developing mutant seeds were narrower in width compared to WT seeds starting from 4 DAP (Figure S5b). This reduced width was more significant at the upper part of the

seed. The mutant phenotype was more severe when seeds were dried, with mutant seeds appearing severely shrunken while WT seeds appeared oval shaped (Figure S5b).

Longitudinal sections of the developing seeds indicated that the mutant endosperm did not develop. No significant difference between mutant and WT seeds was observed at 1 DAP (Figure S7a, f); however, differences became obvious at 4 DAP (Figure S7b,g). Whereas WT seeds were filled with a large

number of endosperm cells, mutant seeds did not exhibit endosperm development and the central part of each seed remained empty. At later developmental stages, mutant seeds enlarged without an endosperm (Figure S7h–j). During the stages, mutant embryos divided but failed to differentiate normally (Figure S7 and S8). Overall, these observations suggest that mutant seeds were defective starting in the early stages of development.

Mutant seeds were defective in syncytial endosperm

Early endosperm development consists of the syncytial stage from 1 to 2 DAP and the cellularization stage at 3 DAP in rice (Lopes and Lar-kins, 1993; Hara *et al.*, 2015; Qi *et al.*, 2020). To examine potential defects in detail, WT and mutant seeds were harvested in the early stages of development (Figure 4). In WT seeds, the endosperm nuclei started to divide at 1 DAP (Figure 4a,g) and at 2 DAP were rapidly dividing and separated by the formation of interzonal phragmoplasts between sister nuclei. This directed the distribution of endosperm nuclei to the peripheries of the endosperm cells (Figure 4b,h). At 3 DAP, the syncytial endosperm was cellularized (Figure 4c,i), as previously reported (Sabelli and Larkins, 2009). In *enl2-2* seeds, a clump of several endosperm nuclei had formed at 1 DAP (Figure 4d,j) and the number of nuclei had slightly increased by 2 DAP. However, these nuclei were not spaced apart and did not migrate to the periphery (Figure 4e,k). At 3 DAP, most mutant endosperm

nuclei had degenerated (Figure 4f,l). In contrast, embryo development did not significantly differ between the mutant and WT during the early developmental stages. Longitudinal sections of the embryos from seeds at 1 to 3 DAP showed that the embryos in the mutant ovaries increased in size in a similar manner as WT embryos and formed globular embryos at 3 DAP (Figure 4m–r).

To study defects in the syncytial nucleus structure of the early endosperm, we performed propidium iodide (PI) staining with whole-mounted developing ovaries and analysed the endosperm nuclei by confocal laser-scanning microscopy. Embryo development appeared similar for WT and *enl2-2* at 3, 8 and 24 HAP (Figure 5 a1, a3, b1, b3, c1, c3, d1, d3, e1, e3, f1 and f3). At 3 HAP, the endosperm nuclei began dividing in both WT and *enl2-2* (Figure 5 a2, a4, b2 and b4). At 8 HAP, the number of WT and *enl2-2* endosperm nuclei was 8 to 16 (Figure 5 c2, c4, d2 and d4) as previously reported (Hara *et al.*, 2015). At 24 HAP, the number of WT endosperm nuclei had significantly increased, with some nuclei migrating to the endosperm periphery (Figure 5 e2, e4). In contrast, *enl2-2* endosperm still contained approximately 10–16 nuclei, forming a clumped structure that failed to migrate (Figure 5 f2,f4). These results indicate that *enl2-2* endosperm nuclei divided three to four times before stopping.

Quantitative RT-PCR analysis of the genes involved in cell cycle and cell division (*CycB1;1, Cyclin A1;1, CDKA1, CDKA2, Cyclin B2;2, OsKRP1, OsKRP3, OsKRP4, OsKRP5* and *OsKRP6*) in the
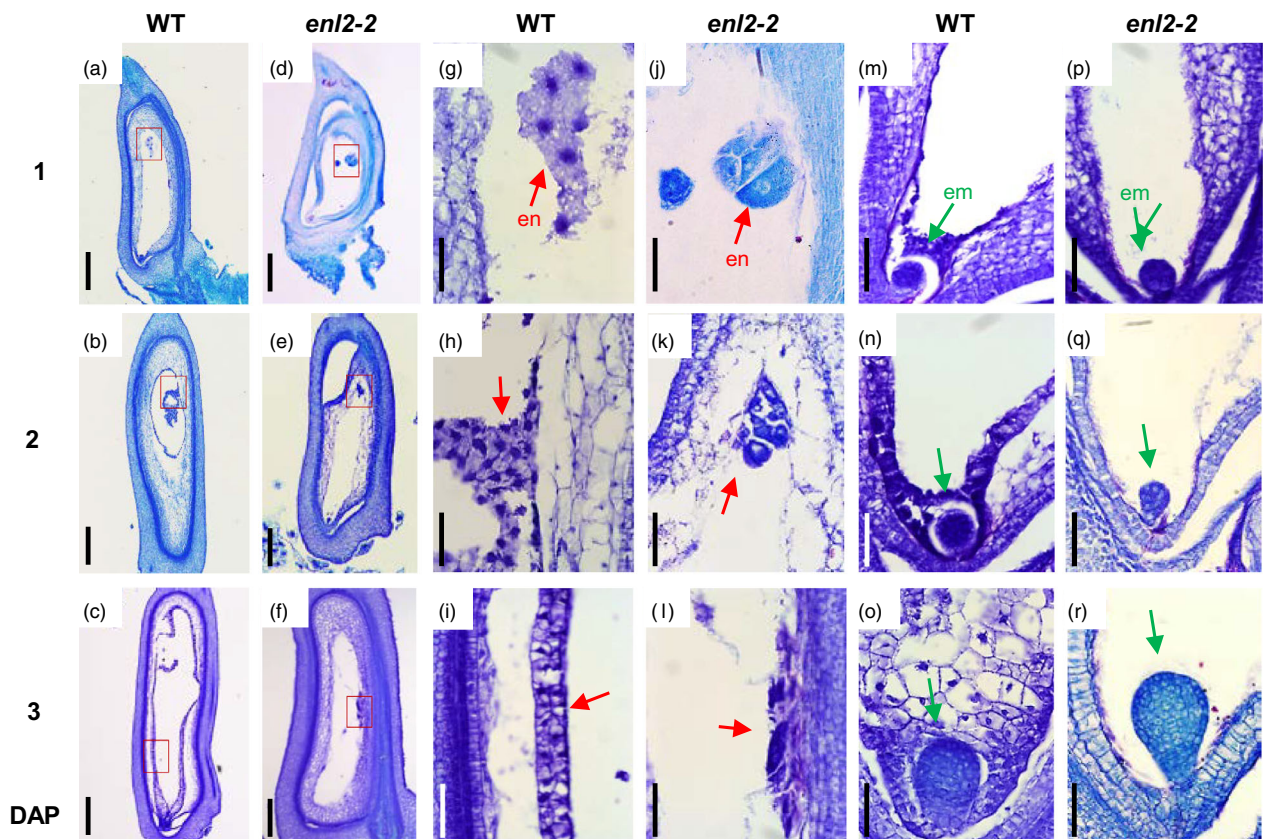

FIGURE 4 Morphological comparisons of developing WT and *enl2-2* endosperm and embryos at 1–3 DAP. (a-f) Developing WT (a-c) and *enl2-2* (d-f) seeds at 1, 2 and 3 DAP. Longitudinal sections of the seeds were stained with toluidine blue. Scale bar, 500 μm. (g-l) Enlarged views of red rectangles in (a-f). Red arrows indicate endosperm (en). Scale bar, 50 μm. (m-r) Developing WT (m-o) and *enl2-2* (p-r) embryos at 1, 2 and 3 DAP. Green arrows indicate embryos (em). Scale bar, 50 μm.
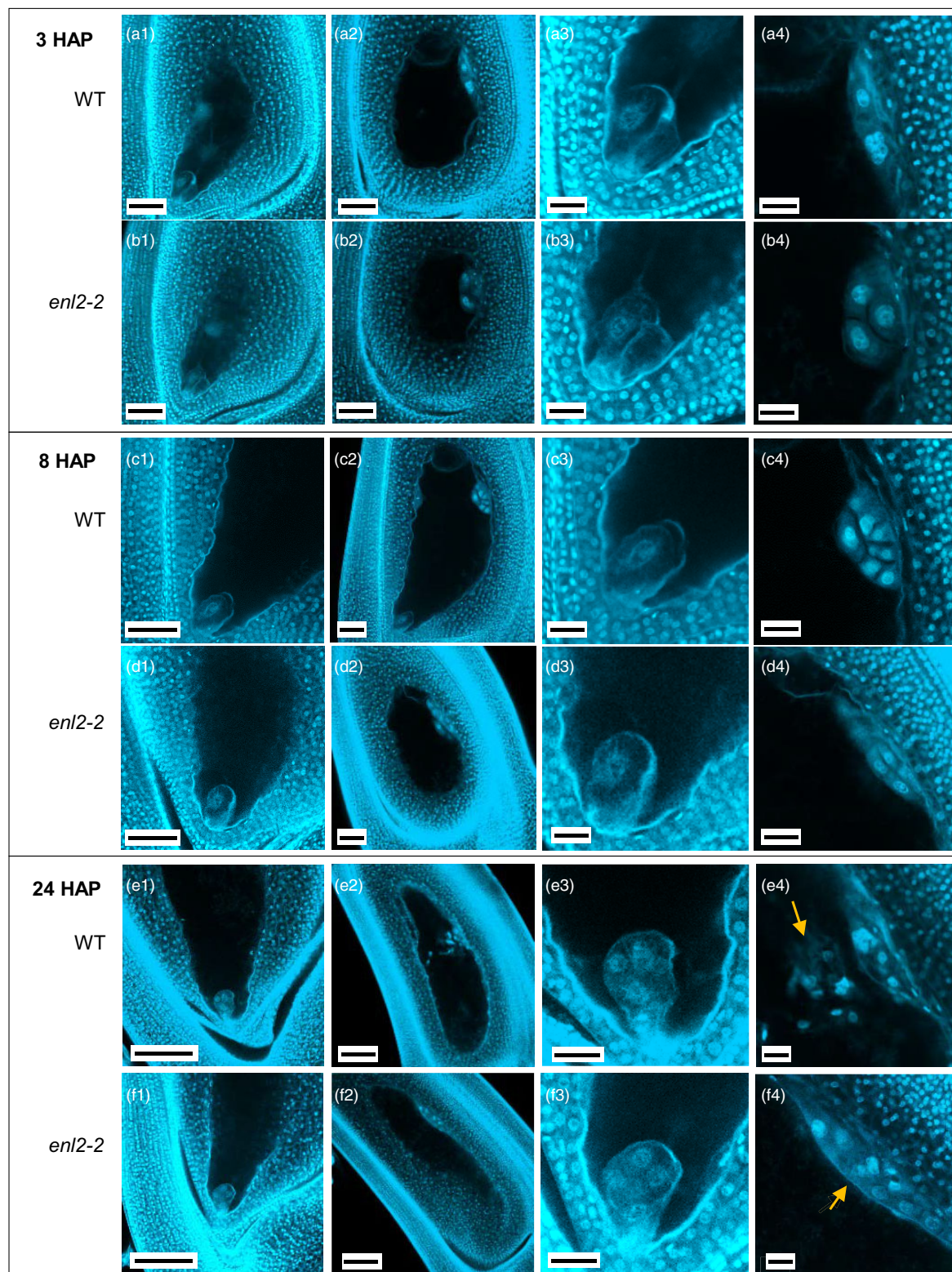
FIGURE 5 Early endosperm and embryo development in WT and *enl2-2* seeds. (a and b) PI staining of whole-mount developing WT (a) and *enl2-2* (b) ovaries at 3 HAP. Developing WT (a1 and a3) and *enl2-2* (b1 and b3) embryos. Developing WT (a2 and a4) and *enl2-2* (b2 and b4) endosperm. Scale bars, 50 μm (a1, a2, b1 and b2); 20 μm (a3, a4, b3 and b4). (c and d) PI staining of whole-mount developing WT (c) and *enl2-2* (d) ovaries at 8 HAP. Developing WT (c1 and c3) and *enl2-2* (d1 and d3) embryos. Developing WT (c2 and c4) and *enl2-2* (d2 and d4) endosperm. Scale bars, 50 μm (c1, c2, d1 and d2); 20 μm (c3, c4, d3 and d4). (e and f) PI staining of whole-mount developing WT (e) and *enl2-2* (f) ovaries at 24 HAP. Developing embryo of WT (e1 and e3) and *enl2-2* (f1 and f3). Developing WT (e2 and e4) and *enl2-2* (f2 and f4) endosperm. Scale bars, 100 μm (e1, e2, f1 and f2); 20 μm (e3, e4, f3 and f4). Arrows indicate critical differences at 24 HAP.

developing seeds at 3 HAP and 24 HAP showed that the expression levels of the genes were not significantly changed in the *enl2-2* mutant (Figure S9). However, the expression of *MADS79* and *MADS89*, which are markers of cellularization, was decreased at 24 HAP (Figure S9), supporting that mutation of *OsCTPS1* caused defects in nuclear spacing rather than mitosis.

The OsCTPS1 protein associates with microtubules

Since the main differences between *enl2-2* and WT endosperm appeared to arise from a lack of nuclei spacing and migration in *enl2-2* endosperm, OsCTPS1 may be involved in the formation of the RMS required for nuclei distribution. To evaluate this hypothesis, we visualized microtubules using anti-tubulin antibodies and stained nuclei with DAPI at 1 DAP. WT endosperm nuclei were evenly spaced by RMSs that radiate the nuclei (Figure 6a). In contrast, *enl2-2* endosperm nuclei were compactly packed, likely due to a reduced amount of associated RMS (Figure 6b). These observations suggest that OsCTPS1 may involve in microtubule organization during endosperm development. To determine whether OsCTPS1 associates with microtubules, we generated transgenic plants expressing the OsCTPS1-sGFP fusion protein. Immunoprecipitation experiments involving leaf extracts mixed with either α-tubulin or β-tubulin antibodies showed that OsCTPS1 binds to both α-tubulin and β-tubulin (Figure 6c). To confirm these interactions, full-length OsCTPS1 cDNA was fused to a Myc tag while α-tubulin and β-tubulin were fused to an HA tag and then co-expressed in the protoplasts prepared from rice callus (Oc) suspension cells. After immunoprecipitation by anti-HA antibodies, the interacting proteins were detected using anti-Myc antibodies. Results of this experiment confirmed that OsCTPS1 interacts with α-tubulin and β-tubulin (Figure 6d), which is consistent with a previous observation that CTPS binds to tubulin in human embryonic kidney cells and that CTPS colocalizes with microtubules (Higgins *et al.*, 2008).

OsCTPS1 transiently forms macromolecular structures in syncytial endosperm

Macromolecular CTPS protein structures have previously been reported in both microorganisms and animals. To evaluate whether OsCTPS1 forms such structures, we constructed the fusion protein OsCTPS1-sGFP. When this fusion protein was expressed in *S. cerevisaiae* and the signal visualized using a fluorescent microscope, one to several rod-shaped macrostructures were present in each cell (Figure 7a). The length of each rod-shaped structure was about 10–50% of the cell diameter, which is similar to native macromolecular CTPS structures previously described in budding yeast. Control cells expressing sGFP alone showed evenly distributed GFP signal in each cell (Figure 7b).

To investigate whether OsCTPS1 forms macrostructures in rice, the OsCTPS1-sGFP fusion protein was co-expressed with NLS-RFP, a nuclear marker, in protoplasts prepared from Oc rice suspension
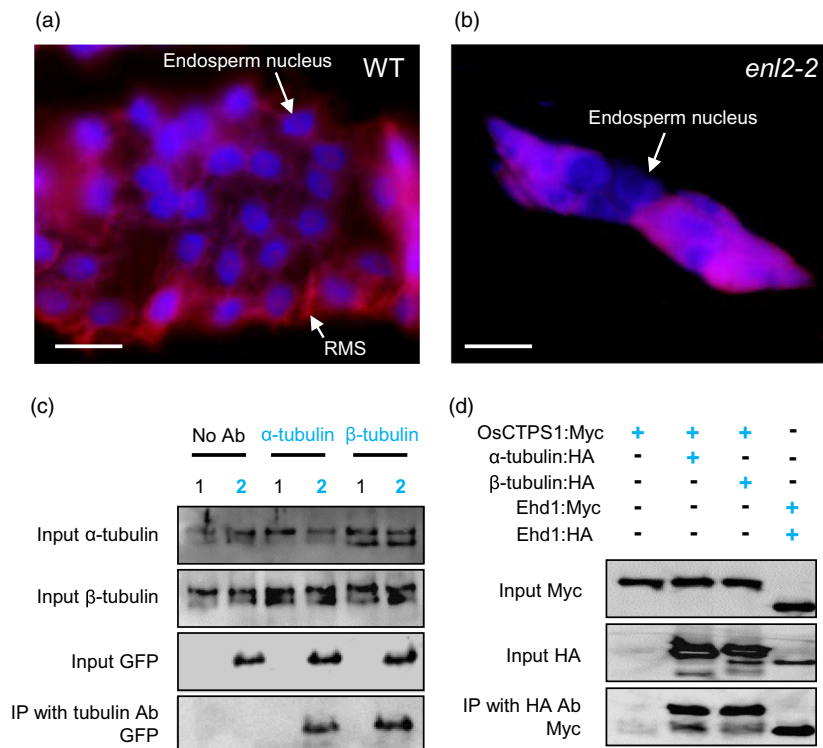

FIGURE 6 The association of OsCTPS1 with microtubules. (a and b) Immunolocalization of β-tubulin in microtubules at 24 HAP. Microtubules were immunolabelled with anti-β-tubulin and the nuclei stained with DAPI (blue) in WT (a) and *enl2-2* (b) endosperm. Scale bar, 20 μm. RMS, radial microtubule system. (c) Immunoprecipitation of α- and β-tubulin using OsCTPS1-GFP. Leaf blades of transgenic plants expressing OsCTPS1-GFP and WT plants were collected for immunoprecipitation assays. After immunoprecipitation with α- or β-tubulin antibodies, samples were detected using GFP antibodies following SDS-PAGE. 1, WT; 2, OsCTPS1-GFP transgenic plants. (d) Co-immunoprecipitation of OsCTPS1 with α- and β-tubulin antibodies. OsCTPS1 was Myc-tagged and α- and β-tubulin were HA-tagged. OsCTPS1-HA and α- or β-tubulin-HA were co-expressed in Oc cell protoplasts. Total protein extracts were immunoprecipitated with anti-HA antibodies, and interaction signals were detected using anti-Myc antibodies following SDS-PAGE.
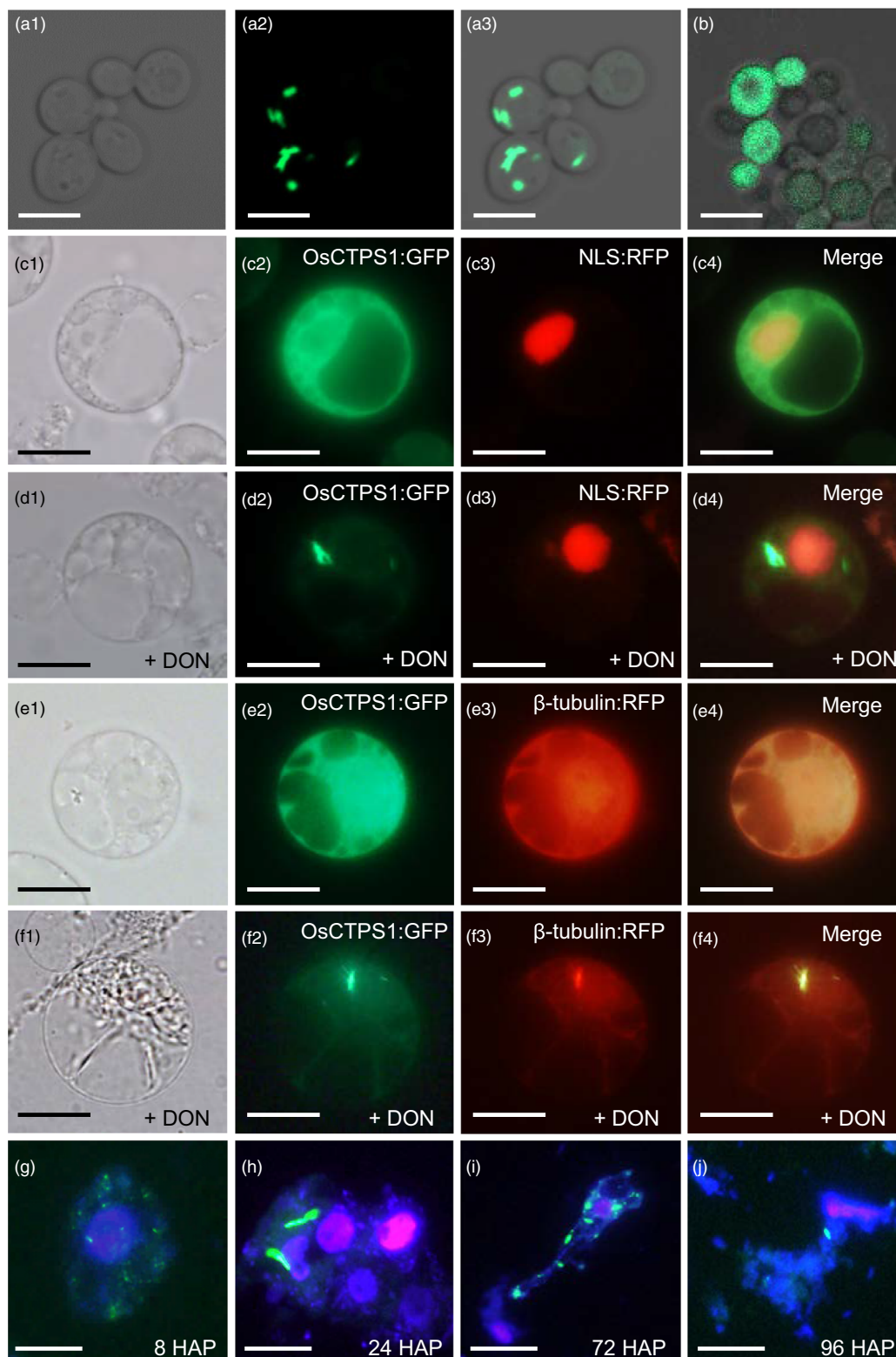
FIGURE 7 Filamentous structures of OsCTPS1 in yeast and rice. (a and b) GFP florescence signal in *S. cerevisiae* expressing OsCTPS1-sGFP (a) and sGFP (b). DIC image (a1), GFP signal (a2) and merged images (a3) of *S. cerevisiae* expressing OsCTPS1-sGFP. Scale bar, 5 μm. (c and d) Subcellular localization of OsCTPS1-GFP in untreated (c) and 4 μg/ml DON-treated (d) rice protoplasts. DIG images of rice protoplasts (c1 and d1), GFP signal (c2 and d2) and merged images of OsCTPS1-GFP and NLS-mRFP (c4 and d4). NLS-mRFP was used as a nuclear marker (c3 and d3). Scale bar, 10 μm. (e and f) Co-localization of OsCTPS1 and β-tubulin. OsCTPS1:GFP and β-tubulin:RFP were co-expressed in untreated (e) or 4 μg/ml DON-treated (f) Oc cells. Rice protoplasts DIG (e1 and f1), GFP signal (e2 and f2), RFP signal (e3 and f3) and merged images of OsCTPS1-GFP and β-tubulin:mRFP (e4 and f4). Scale bar, 10 μm. (g-j) Filamentous structures of OsCTPS1 in developing endosperm. Fluorescence of developing endosperm at 8 HAP (g), 24 HAP (h), 72 HAP (i) and 96 HAP (j) from transgenic plants expressing OsCTPS1-GFP. Scale bar, 10 μm.

cells. Visualization of OsCTPS1-sGFP signal revealed that OsCTPS1 is evenly distributed between the cytoplasm and the nucleus (Figure 7c). However, when Oc cell protoplasts were treated with the glutamine analog 6-diazo-5-oxo-L-norleucine (DON), the GFP signal became condensed and formed macromolecular structures (Figure 7d), which is similar to results involving DON-induced formation of CTPS filamentous structures in *Drosophila* and human cells (Chen *et al.*, 2011). We also observed co-localization of OsCTPS1-sGFP and β-tubulin-RFP signals in normal and DON treatment conditions (Figure 7e,f). These results support the association of OsCTPS1 and tubulins to form microtubules.

To study whether these macromolecular structures are related to the phenotypes observed in *osctps1* mutants, we generated transgenic rice plants that expressing OsCTPS1-sGFP protein under the control of the constitutive maize promoter *Ubi1*. Since the mutant phenotype was most prominent in the endosperm during early developmental stages, we analysed developing endosperms at 8, 24, 72 and 96 HAP. A large number of GFP signal puncta were observed in endosperm cytoplasm at 8 HAP (Figure 7g). In addition, long macromolecular structures were detected in the cytosol at 24 HAP (Figure 7h) while short, rod-like structures were visible at 72 HAP (Figure 7i). Moreover, the GFP signal had almost completely diminished at 96 HAP (Figure 7j). These result indicated that OsCTPS1 transiently forms macromolecular structures during the early stage of endosperm development when *enl2* displayed the endosperm defect phenotypes.

Overexpression of *OsCTPS1* improves grain yield

In order to see whether increased expression of *OsCTPS1* promotes endosperm development, *OsCTPS1*-overexpressing plants were produced in which *OsCTPS1* expression was controlled by the maize *ubiquitin* promoter. Out of six independently transformed plants, we selected two lines (#2 and #6) that expressed *OsCTPS1* at high levels for further examination (Figure 8a). The typical grain size, length, width, thickness and 1000-grain weight of both overexpression lines was greater than that of WT (Figure 8b-f). Most agronomic traits of *OsCTPS1*-overexpressing plants were similar to WT, except for plant height, which was slightly decreased in transgenic plants (Figure S10).

When the endosperms were observed at 60 HAP, more endosperm cells had formed in the grains of the transgenic plants than in WT grains (Figure 8g-l). These results suggest that the increased expression of *OsCTPS1* enhances nuclear division in the endosperm, resulting in increased grain size.

Discussion

Rice is a major food crop in many regions of the world (Lo *et al.*, 2020); thus, as the world population continues to grow, increasing rice grain yield is important. Grain yield is determined by several factors including grain size, panicle number per plant, grain number per panicle and fertility (Xing and Zhang, 2010; Lo *et al.*, 2020; Yang *et al.*, 2020). In addition, several studies have indicated that spikelet hull size depends on both cell proliferation and expansion (Lyu *et al.*, 2020; Yang *et al.*, 2020). Although endosperm development plays a major role in controlling the quality and quantity of rice grains, the mechanisms underlying the early stages of cereal endosperm development remain largely unknown (Qi *et al.*, 2020).

We identified rice mutants defective in the early stages of endosperm development. Null *OsCTPS1* mutants showed halted

nuclear division at 24 HAP during syncytial endosperm formation. Endosperm nuclei in *osctps1* plants did not migrate to the periphery of the cell and degenerated, resulting in the loss of endosperm. This endosperm defect in *enl2* occurred earlier than defects associated with other rice endosperm mutants. Among the several genes that have been identified as playing important roles during endosperm development, *OsLFR* was the gene with the earliest known function. Mutants defective in OsLFR function start to display endosperm defects at 32 HAP, when they possess fewer free nuclei at the periphery of the endosperm than WT plants (Qi *et al.*, 2020). Since our *enl2* mutant showed endosperm defects at 24 HAP, *OsCTPS1* seems to function at least 8 h before *OsLFR*. The nuclei from *oslfr* mutants were able to migrate to the periphery of endosperm cells, whereas *enl2* endosperm nuclei did not migrate, also supporting the earlier function of *OsCTPS1*.

The *enl2* mutants showed endosperm defects earlier than the mutants with mutations in genes associated with cellularization, including knock-down mutants *CycB1;1* that exhibit issues with cell wall formation (Guo *et al.*, 2010) and mutants lacking *MADS78* or *MADS79* that display precocious endosperm cellularization (Paul *et al.*, 2020). The *enl2* mutants also showed altered phenotypes before the mutants with altered mitotic chromosomal segregation or endoreduplication arising from defects in *enl1*, *NF-Y* and *OsCCS52A* (Hara *et al.*, 2015; Su'udi *et al.*, 2012; Sun *et al.*, 2014).

Our *enl2* mutants also displayed enlarged embryos, which is consistent with previous observations associating enlarged embryos with other endosperm mutants (Guo *et al.*, 2010; Hara *et al.*, 2015; Nagasawa *et al.*, 2013; Su'udi *et al.*, 2012; Sun *et al.*, 2014; Yang *et al.*, 2013). These increases in embryo size appear to be linked with the absence of the endosperm. Endosperm-specific suppression of cell cycle inhibition has been shown to cause endosperm defects and increases in embryo size (Guo *et al.*, 2010), and interactions between the embryo and endosperm at interface tissues appear to play critical roles in controlling embryo size (Nagasawa *et al.*, 2013). Although the embryos were large in our *enl2* mutant seeds, they developed normally, including during the early developmental stages, indicating that the endosperm is not needed for early embryo development. Whereas the overall embryo structure was normal in *enl2-1*, *enl2-2* embryos were occasionally defective and seeds sometimes failed to germinate, indicating that this null mutation caused more severe phenotypes than the less severe mutation in *enl2-1*.

The rice genome contains six CTPS genes, of which two (*OsCTPS3* and *OsCTPS4*) were expressed at very low levels in all organs tested. The remaining four CTPS genes were ubiquitously expressed in various tissues. This redundancy may contribute to the lack of apparent phenotypic changes at most developmental stages in the *enl2* mutants. However, *enl2* mutants showed defects in nuclear division in the endosperm, suggesting that more than one CTPS gene is needed for rapid nuclear division when a large number of nucleotides are needed for DNA synthesis.

Unlike the distant spacing of nuclei in WT endosperm, the nuclei in *enl2* endosperm were closely packed and appeared to clump, which appeared to arise due to a lack of sister nuclei separation by microtubules in the endosperm. In addition, *enl2* endosperm nuclei failed migration to the cell periphery. Since this nuclei movement to the sac periphery is likely mediated by microtubules, the major defect in *enl2* mutant endosperm may be due to an insufficient amount of functional microtubules. We
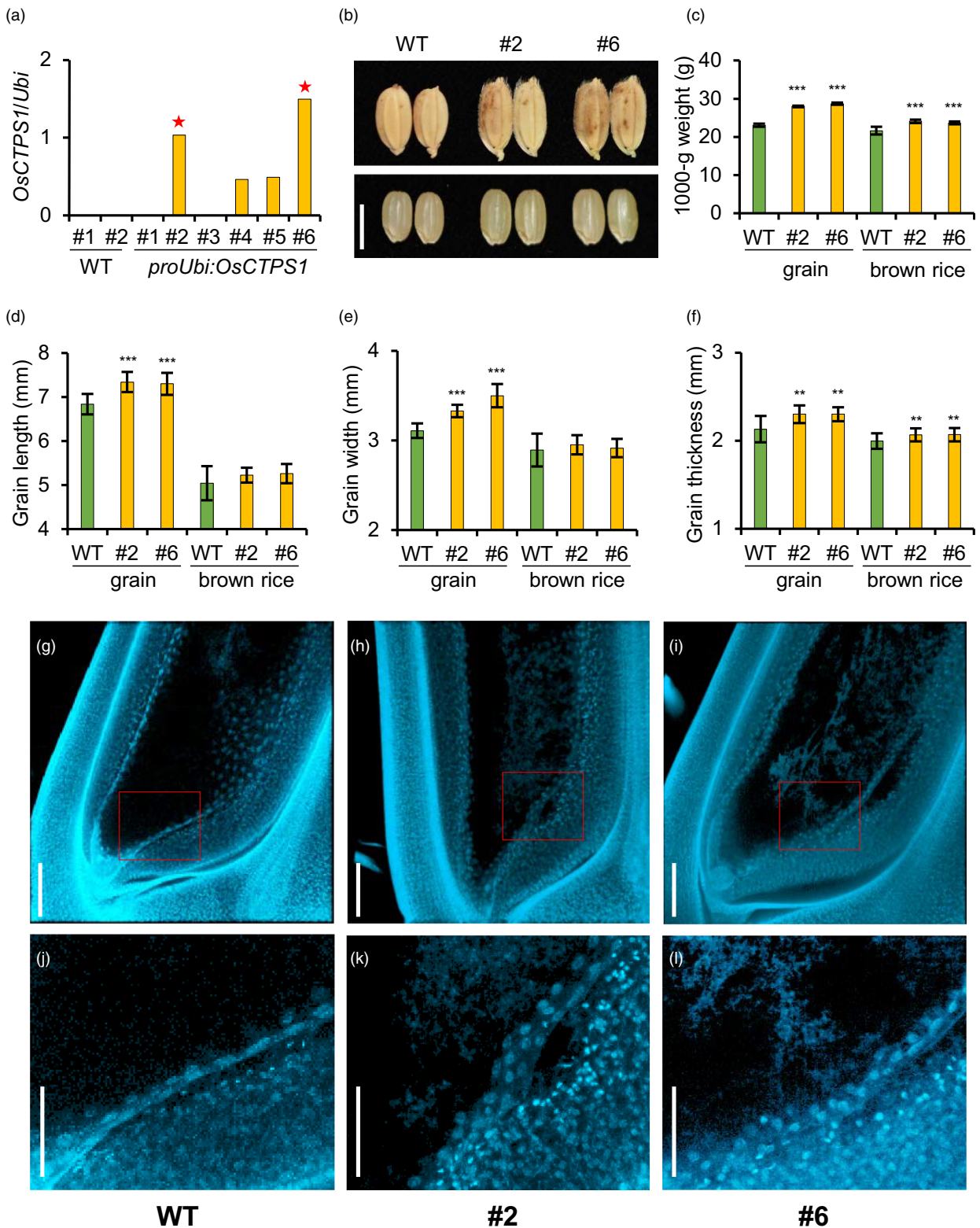
FIGURE 8 Characterization of *OsCTPS1*-overexpressing plants. (a) *OsCTPS1* expression levels in *OsCTPS1*-overexpressing transgenic plants. RNA samples were collected from seedling leaf blades. Numbers indicate individual transgenic plants. (b) Phenotype of *OsCTPS1*-overexpressing and WT plant grains. Scale bar, 5 mm. (c) 1000-grain weight of *OsCTPS1*-overexpressing plants compared with WT. $n = 4$. Statistical significance is indicated by *** ($P < 0.001$). (d) Grain length in *OsCTPS1*-overexpressing plants compared to WT. $n = 10$. Statistical significance is indicated by *** ($P < 0.001$). (e) Grain width in *OsCTPS1*-overexpressing plants compared to WT. $n = 10$. Statistical significance is indicated by *** ($P < 0.001$). (f) Grain thickness in *OsCTPS1*-overexpressing plants compared to WT. $n = 10$. Statistical significance is indicated by *** ($P < 0.001$) and **($P < 0.05$). (g-i) Z-stack images obtained by confocal laser-scanning microscopy of WT (g) and *OsCTPS1*-overexpressing plants (h and i). Scale bar, 100 μm. (j-l) Enlarged images of red boxes in Figure g-i. Scale bars, 50 μm.

showed that OsCTPS1 interacts with tubulin proteins, supporting the possibility that OsCTPS1 is involved in microtubule function. It was previously reported that plant microtubules associate with several proteins during endosperm development (Huang *et al.*, 2019; Pignocchi *et al.*, 2009). For example, endosperm defective1 (EDE1) is a microtubule-associated protein that is essential for microtubule function during mitosis and cytokinesis in *Arabidopsis* endosperm and embryo (Pignocchi *et al.*, 2009). In addition, the kinesin-14 subfamily protein *VKS1* colocalizes with microtubules to enable free nuclei migration in the developing endosperm in maize (Huang *et al.*, 2019).

Cells of transgenic plants expressing OsCTPS1-GFP fusion proteins exhibit rod-shaped macromolecular structures. Although transient expression of *Arabidopsis* CTPS in *Nicotiana benthamiana* protoplasts produced aggregates, these clusters did not form uniformly organized structures (Daumann *et al.*, 2018). Furthermore, *Arabidopsis* CTPS did not form macromolecular structures when expressed in *S. cerevisiae*. In contrast, we showed that rice OsCTPS1 formed macromolecular structures in *S. cerevisiae* and in stably transformed plants, indicating that CTPS transiently forms macromolecular structures.

Although we used the constitutively expressed *Ubi* promoter, macromolecular structures were only detected in endosperm cells undergoing rapid nuclear division, indicating that such division may be a requirement for OsCTPS1 macromolecular structure formation. CTPS macromolecular structures specifically formed at a stage when large amounts of CTP were needed, suggesting that these structure increase enzyme activities. Our observations are consistent with previous reports indicating that CTPS macromolecular structures in animals are formed at specific stages of development (Liu, 2016). In *Drosophila*, these structures are observed in early-stage neuroblasts of the larval central nervous system (Aughey *et al.*, 2014). In mice, such structures preferentially arise in fast-growing cells and in the axons of rat neurons (Noree *et al.*, 2010). The requirement of a large number of macromolecular CTPS structures during rapid nuclear division thus appears to be evolutionarily conserved in both animals and plants.

The function of CTPS filaments remains under debate (Liu, 2016). Cells may form these filamentous macromolecular structures to store inactive enzymes so they can be released when required. This idea is supported by the observation that CTPS polymerization inhibits CTPS activity in bacteria. In addition, destabilization of the active tetrameric arrangement to form dimers increases filament formation in *S. cerevisiae*, suggesting that the filaments are comprised of inactive CTPS dimers (Noree *et al.*, 2014). In contrast, CTPS polymerization increases catalytic activity in human cells (Lynch *et al.*, 2017). These varied regulatory mechanisms may arise from structural differences between microbes and human cells observed using cryo-electron microscopy (Lynch *et al.*, 2017). In this study, we provided a possibility that CTPS filaments may involve in nuclei spacing by interacting with microtubules.

Experimental procedures

Plant materials and growth conditions

The endospermless mutant *enl2-1* (Line no. PFG_1C-15623) was identified from a mutant population of *Oryza sativa* var. *japonica* cultivar Hwayoung. Deletion mutants were generated in the *japonica* rice cultivar *Oryza sativa* var. *japonica* cultivar Nipponbare. Seeds were either germinated on 1/2 Murashige and Skoog (MS) medium containing 3% sucrose or directly in soil as previously reported (Yi and An, 2013). Plants were grown in a controlled growth room (14 h light, 28°C/10 h dark, 22°C; humidity approximately 60%) or a paddy in Yongin, Korea, as previously described (Cho *et al.*, 2016).

5-Ethynyl-2'-deoxyuridine staining

S-phase cells were visualized by 5-ethynyl-2'-deoxyuridine (EdU) staining as previously reported (Kotogány *et al.*, 2010; Yoon *et al.*, 2020). Plants grown on MS medium were transferred to new MS medium containing 10 μM EdU and incubated for 4 h. Samples were then fixed for 1 h in 4% paraformaldehyde in PBS (pH 7.2) and permeabilized in a PBS solution containing 0.5% Triton X-100 for 30 min. Next, samples were incubated for 30 min in an EdU detection cocktail (C10338, Click-it EdU Alexa Fluor 555; Invitrogen). Images were obtained using the RFP channel of a LSM 800 confocal microscope (Carl Zeiss, Oberkochen, Germany).

Map-based cloning

Homozygous *enl2-1* mutant plants (male parent) were crossed with the *indica* type cultivar Milyang 23 (female parent). F_1 hybridity was confirmed using the polymorphic SSR markers R1M7 and R7M7 (Shen *et al.*, 2004). F_2 seeds harvested from 25 F_1 plants were de-husked for the selection of mutant and normal seeds. For bulked segregant analysis, 20 mutants and 20 normal seeds were grown on MS agar media. Genomic DNA was extracted from each resulting plant using the CTAB method and the same amount of genomic DNA from each of four plants was pooled into one tube, resulting in five tubes for mutant seeds and another five tubes for normal seeds. The pooled DNA was genotyped using SSR markers distributed across 12 chromosomes. For fine mapping, normal and mutant seeds were germinated on MS media and genomic DNA isolated from each seedling using a simple, non-toxic DNA preparation protocol (Kim *et al.*, 2016). Individual plants were genotyped by RM9 and R1M30 markers and only recombinants between these two markers further analysed. New markers, including InDel type polymorphic markers and SNP markers, were developed using reference genomic sequences of *japonica* (Nipponbare IRGSP 1.0) and *indica* rice variants (93-11 variety). All of the primers used for fine mapping are listed in Table S1.

Co-immunoprecipitation (Co-IP) analysis

Co-IP assays were performed as previously described (Cho *et al.*, 2016; Yoon *et al.*, 2017). Briefly, fusion proteins were co-expressed in rice Oc cell protoplasts then total proteins extracted in IP buffer [75 mM NaCl, 50 mM Tris-HCl (pH 7.5), 5 mM EDTA, 1% Triton X-100, 1 mM dithiothreitol, 1 mM phenylmethanesulfonyl fluoride, 2 mM NaF, 20 μM MG132, protease inhibitor cocktail (Roche)]. Expressed proteins were immunoprecipitated using anti-HA mouse monoclonal antibodies (12CA5; Roche) or anti-Myc mouse monoclonal antibodies (#2276; Cell Signaling) conjugated with A and G agarose beads (Millipore, Billerica, MA, http://www.emdmillipore.com). For protein detection, horseradish peroxidase (HRP)-conjugated anti-HA monoclonal antibody (#2999; Cell Signaling) or anti-Myc monoclonal antibody (#2040; Cell Signaling) were used.

CTP synthase activity assay

Full-length cDNA encoding OsCTPS1 was amplified using the primer pairs listed in Table S2. The cDNA was cloned into the *Bam*HI and *Xho*I sites of the 6X His-fusion protein expression

vector pET28a(+). The bacterial strain *E. coli* BL21 (DE3) was used as a host for recombinant protein expression. The N-terminal 6X His-tagged proteins were purified using nickel-nitrilotriacetic acid (Ni-NTA) agarose beads (QIAGEN, USA; https://www.qiagen.com) according to the manufacturer's instructions. The CTP synthase activity was determined by comparing changes in extinction coefficients of UTP and CTP (182 M/cm and 1520 M/cm, respectively) at 291 nm. This assay for measuring for CTP synthase activity examines the relative conversion of UTP to CTP by the same concentration of purified OsCTPS1-WT or OsCTPS-N81I. The standard reaction mixture was 0.1 ml total and consisted of 50 mM Tris-HCl (pH 8.0), 10 mM MgCl$_2$ and 10 mM β-mercaptoethanol with final substrate concentrations of 2 mM L-glutamine, 2 mM ATP, 2 mM UTP, 0.1 mM GTP and an appropriate dilution of purified protein, as previously described (Chang *et al.*, 2007). During the reaction mixture incubation at 37°C, the UV absorption was measured every 5 or 10 min for 1 h total. At least three independent replicates were conducted for each assay each involving three biological replicates.

Vector construction and plant transformation

To generate transgenic plants expressing OsCTPS1-sGFP, full-length *OsCTPS1* cDNA was amplified by PCR using the primers listed in Table S2 and then digested with the restriction enzymes *Bsi*WI and *Spe*I and inserted into the binary vector pGA3427 under the control of the maize *ubiquitin 1* promoter (Kim *et al.*, 2009). To generate p*OsCTPS1-GUS* transgenic plants, a 2.55-kb fragment of the *OsCTPS1* promoter region was amplified using the primer pair listed in Table S2. Genomic DNA from 'Nippon-bare' rice was used as a template. The amplified promoter fragment was inserted between the *Hpa*I and *Xho*I restriction sites of the pGA3383 binary vector carrying the *GUS* coding sequence followed by the *nopaline synthase* terminator (Kim *et al.*, 2009). *osctps1* knockout plants were generated in the 'Nipponbare' background using CRISPR/Cas9 with the CRISPR/Cas9 vector previously described in (Cho *et al.*, 2018). The spacer sequence 5'-GGCACCTTACCTTAACACAGATGC-3' was cloned into the entry vector pOs-sgRNA to monitor sgRNA expression. The resulting recombinant entry vector, pOs-sgRNA, was then cloned into the destination vector pH-Ubicas9-7 using the GatewayTM system (Miao *et al.*, 2013). Binary vectors were introduced into *Agrobacterium tumefaciens* LBA4404 using the freeze–thaw method (An et al., 1988) and rice transformation via *Agrobacterium*-mediated co-cultivation performed as previously reported (Jeon *et al.*, 2000). For genotyping, genomic DNA was extracted from leaf blades and the CRISPR/Cas9 target region sequenced using primers listed in Table S2.

RNA isolation and quantitative RT-PC analysis

Total RNA was isolated from freshly collected plant tissue using RNAiso Plus (TaKaRa, Shiga, Japan; http://www.takarabio.com). RNA samples were qualified using a Nano-Drop 2000 (Thermo Scientific, Wilmington, DE, USA; http://www.nanodrop.com) with expected 260/280 nm ratios of >1.8, as described previously (Cho *et al.*, 2018). First-strand cDNA synthesis was performed with 2 μg of total RNA, Moloney murine leukaemia virus reverse transcriptase (Promega, Madison, WI; http://www.promega.com), RNasin® Ribonuclease Inhibitor (Promega), oligo (dT) 18 primers and dNTPs. Quantitative RT-PCR was performed using synthesized cDNA and SYBR Green I Prime Q-Master mix (GENETBIO, Daejeon, Republic of Korea) and a Rotor-Gene Q system qRT-PCR machine (Corbett Research, Sydney, Australia; http://www.corbettlifescience.com), as previously described (Cho *et al.*, 2018). Rice *Ubi1* was used as an internal control. The primer pairs for quantitative RT-PCR are listed in Table S2.

Histochemical analysis and GUS assay

Following vacuum infiltration, seed samples were fixed in FAA (3.7% formaldehyde, 5% acetic acid, 50% ethanol) solution and incubated at 4°C overnight. Samples were then dehydrated using a graduated ethanol series (50, 70, 90 and 100%) and then treated with a t-butyl alcohol series and infiltrated with paraffin. Next, tissues were cut to a thickness of 10 μm with a microtome (model 2165; Leica Microsystems, http://www.leica-microsystems.com/) and the cut samples attached overnight to a coated slide on a 60°C hotplate. Samples were then rehydrated with 100% HistoChoice for clearing, an ethanol series (100, 70, 50 and 30%), and distilled water as previously described (Yoon *et al.*, 2017). Samples were stained with toluidine blue and protected with a cover slide then observed under a BX61 microscope (Olympus, http://www.olympus-global.com/en/). Histochemical GUS staining was performed as previously described (Pasriga *et al.*, 2018; Yoon *et al.*, 2014; Yoon *et al.*, 2019). After vacuum infiltration for 60 min, samples were incubated for 8 h at 37°C in a GUS staining solution [100 mM sodium phosphate, 5 mM potassium ferricyanide, 5 mM potassium ferrocyanide, 0.5% Triton X-100, 10 mM EDTA (pH 8.0), 0.1% X-gluc (5-bromo-4-chloro-3-indolyl-β-D-glucuronic acid/cyclohexylammonium salt), 2% DMSO, 5% methanol]. To remove chlorophyll, samples were incubated sequentially in 70% and then in 95% ethanol at 60°C. GUS-stained samples were then soaked for 60 min at room temperature in VISKOL clearing reagent (Phytosys LLC, New Brunswick, NJ, http://visikol.com/). After sectioning samples to a thickness of 10 μm, GUS activity was observed using a BX61 microscope.

Whole-mount developing caryopses observation

Previously published protocols were followed with some modifications (Hara *et al.*, 2015; Qi *et al.*, 2020). Developing caryopses were fixed in FAA (3.7% formaldehyde, 5% acetic acid, 50% ethanol) solution and incubated at 4°C overnight. After fixation, the samples were hydrated with an ethanol series (70%, 50% and 30% for 30 min each) and washed with PBS (0.9% NaCl, 50 mM phosphate buffer, pH 7.4) for 30 min. Next, samples were treated with RNase A (100 μg/ml) at 37°C overnight and then stained with PI (5 μg/ml) at 4°C overnight in the dark. After staining, samples were washed with PBS and dehydrated using an ethanol series (30%, 50%, 70%, 80%, 90% and 100% for 30 min each) and washed twice with absolute ethanol for 30 min per wash. After dehydration, the samples were infiltrated with a methanol–methyl salicylate series [2:1, 1:1 and 1:2 (vol/vol) for 1 h each] and then incubated in methyl salicylate three times for 1 h per incubation then kept at 4°C overnight. Whole-mount developing caryopses were observed using excitation/emission wavelengths of 543 nm and 550–630 nm with a LSM 800 confocal microscope (Carl Zeiss, Oberkochen, Germany).

Immunofluorescence localization

Experiments were performed based on a modified version of a previously published protocol (Pignocchi *et al.*, 2009). To performed immunofluorescence localization, developing seed

samples were fixed in 4% (w/v) paraformaldehyde in microtubule-stabilizing buffer/DMSO (MTSB; 50 mM PIPES, 5 mM EGTA and 5 mM MgCl$_2$ in 5% DMSO, pH 6.7 to 7.0). Samples were then dehydrated by an ethanol series (50, 70, 90 and 100%) and then treated with a t-butyl alcohol series and infiltrated with paraffin. After embedding, samples were cut to a thickness of 10 μm with a microtome and sectioned samples rehydrated and then digested with 2% (w/v) driselase (Sigma-Aldrich) for 30 min at room temperature. Next, samples were permeabilized with 1% (v/v) Triton X-100 in 10% DMSO-MTSB for 30 min at room temperature. Samples were blocked with 1% (w/v) BSA in MTSB for 1 h at room temperature and incubated with an anti-β-tubulin polyclonal antibody (#PA5-16863; Invitrogen) diluted 1:50 in 3% (w/v) BSA in MTSB at 4°C overnight. After washing with MTSB buffer, samples were incubated in Alexa Fluor 594 goat anti-rabbit IgG (H + L) highly cross-adsorbed secondary antibody (#A11037; Invitrogen) at a 1:300 dilutions in 3% (w/v) BSA in MTSB. DNA was stained with NucBlue® Fixed Cell ReadyProbes® Reagent (#R37606; Invitrogen). Samples were observed using a BX61 microscope (Olympus) with 360 to 370 nm (excitation) and 420 to 460 nm (emission) for DNA detection and 488 nm (excitation) and 610 nm (emission) for β-tubulin signal detection.

Yeast expression assay

To express OsCTPS1 in yeast, the corresponding full-length cDNA was amplified by PCR using the primers listed in Table S2. The cDNA fragment was then inserted into the pPS808 vector (Addgene, plasmid #8856) containing a GFP coding sequence. Haploid *Saccharomyces cerevisiae* YM4271 cells were transformed using a modified lithium acetate transformation protocol (Cho *et al.*, 2016). Transformants were grown on minimal medium that lacking uracil for selection. Fluorescence was detected using a filter-equipped microscope (BX61; Olympus) under bright field or GFP channels.

Statistical analyses

The P values were calculated by using one-way analysis of variance (ANOVA; Tukey HSD test) for the test groups with R program (Cohen and Cohen, 2008).

Conflict of interest

The authors declare no conflict of interest.

Author contributions

J.Y., L.-H.C., S.-R.K and G.A. designed the project; J.Y., L.-H.C., S.-R.K, W.T., X.P., R.P., S.M., W.-J.H., H.J. performed experiments; K.-H.J., J.-S.J. and G.A. analysed and interpreted the data; J.Y., L.-H.C., S.-R.K and G.A. wrote the paper with significant input from all authors.

References

An, G., Ebert, P.R., Mitra, A. and Ha, S.B. (1988) Binary vectors. *Plant Mol Biol Manual*, **A3**, 1–19.

An, S., Kumar, R., Sheets, E.D. and Benkovic, S.J. (2008) Reversible compartmentalization of de novo purine biosynthetic complexes in living cells. *Science*, **320**, 103–106.

Aughey, G.N., Grice, S.J., Shen, Q.J., Xu, Y., Chang, C.C., Azzam, G., Wang, P.Y. *et al.* (2014) Nucleotide synthesis is regulated by cytoophidium formation during neurodevelopment and adaptive metabolism. *Biol. Open*, **3**, 1045–1056.

Bennett, M.D., Smith, J.B. and Barclay, I. (1975) Early seeds development in the Triticeae. *Philos. Trans. R. Soc. Lond., B. Biol. Sci.* **272**, 199–227.

Carcamo, W.C., Satoh, M., Kasahara, H., Terada, N., Hamazaki, T., Chan, J.Y.F., Yao, B. *et al.* (2011) Induction of cytoplasmic rods and rings structures by inhibition of the CTP and GTP synthetic pathway in mammalian cells. *PLoS One*, **6**, e29690.

Chang, Y.-F., Martin, S.S., Baldwin, E.P. and Carman, G.M. (2007) Phosphorylation of human CTP synthetase 1 by protein kinase C: identification of Ser^{462} and Thr^{455} as major sites of phosphorylation. *J. Biol. Chem.* **282**, 17613–17622.

Chen, K., Zhang, J., Tastan, O.Y., Deussen, Z.A., Siswick, M.Y. and Liu, J.L. (2011) Glutamine analogs promote cytoophidium assembly in human and *Drosophila* cells. *J. Genet. Genom.* **38**, 391–402.

Cho, L.H., Yoon, J., Pasriga, R. and An, G. (2016) Homodimerization of Ehd1 is required to induce flowering in rice. *Plant Physiol.* **170**, 2159–2171.

Cho, L.H., Yoon, J., Wai, A.H. and An, G. (2018) *Histone Deacetylase 701* (*HDT701*) induces flowering in rice by modulating expression of *OsIDS1*. *Mol. Cells*, **41**, 665–675.

Choi, M.G. and Carman, G.M. (2007) Phosphorylation of human CTP synthetase 1 by protein kinase A: identification of Thr^{455} as a major site of phosphorylation. *J. Biol. Chem.* **282**, 5367–5377.

Cohen, Y. and Cohen, J.Y. (2008) *Analysis of variance, in statistics and data with R: An applied approach through examples*. Chichester, UK: John Willey & Sons Ltd. https://doi.org/10.1002/9780470721896.

Daumann, M., Hickl, D., Zimmer, D., Detar, R.A., Kunz, H.H. and Mohlmnn, T. (2018) Characterization of filament-forming CTP synthases from *Arabidopsis thaliana*. *Plant J.* **96**, 316–328.

Guo, J., Wang, F., Song, J., Sun, W. and Zhang, X.S. (2010) The expression of *Orysa;CycB1;1* is essential for endosperm formation and causes embryo enlargement in rice. *Planta*, **231**, 293–303.

Hara, T., Katoh, H., Ogawa, D., Kagaya, Y., Sato, Y., Kitano, H., Nagato, Y. *et al.* (2015) Rice SNF2 family helicase ENL1 is essential for syncytial endosperm development. *Plant J.* **81**, 1–12.

Higgins, M.J., Loiselle, D., Haystead, T.A. and Graves, L.M. (2008) Human cytidine triphosphate synthetase 1 interacting proteins. *Nucleosides Nucleotides Nucleic Acids*, **27**, 850–857.

Hong, S.K., Kitano, H., Satoh, H. and Nagato, Y. (1996) How is embryo size genetically regulated in rice. *Development*, **122**, 2051–2058.

Huang, Y., Wang, H., Huang, X., Wang, Q., Wang, J., An, D., Li, J. *et al.* (2019) Maize VKS1 regulates mitosis and cytokinesis during early endosperm development. *Plant Cell*, **31**, 1238–1256.

Iben, L., Martin, W., Jensen, K.F., Johansson, E. and Harris, P. (2011) Structure of the dimeric form of CTP synthase from *Sulfolobus solfataricus*. *Acta Crystallogr. Sect. F. Struct. Biol. Cryst. Commun.* **F67**, 201–208.

Ingerson-Mahar, M., Briegel, A., Werner, J.N., Jensen, G.J. and Gitai, Z. (2010) The metabolic enzyme CTP synthase forms cytoskeletal filaments. *Nat. Cell Biol.* **12**, 739–746.

Jeon, J.-S., Lee, S., Jung, K.-H., Jun, S.-H., Jeong, D.-H., Lee, J., Kim, C. *et al.* (2000) T-DNA insertional mutagenesis for functional genomics in rice. *Plant J.* **22**, 561–570.

Ji, H.-S., Chu, S.-H., Jiang, W., Cho, Y.-I., Hahn, J.-H., Eun, M.-Y., McCouch, S.R. *et al.* (2006) Characterization and mapping of a shattering mutant in rice that corresponds to a block of domestication genes. *Genetics*, **173**, 995–1005.

Kim, S.R., Lee, D.Y., Yang, J.I., Moon, S. and An, G. (2009) Cloning vectors for rice. *J. Plant Biol.* **52**, 73–78.

Kim, S.R., Yang, J., An, G. and Jena, K.K. (2016) A simple DNA preparation method for high quality polymerase chain reaction in rice. *Plant Breed. Biotech.* **4**, 99–106.

Kotogány, E., Dudits, D., Horváth, G.V. and Ayaydin, F. (2010) A rapid and robust assay for detection of S-phase cell cycle progression in plant cells and tissues by using ethynyl deoxyuridine. *Plant Methods*, **6**, 5.

Kurata, N., Miyoshi, K., Nonomura, K., Yamazaki, Y. and Ito, Y. (2005) Rice mutants and genes related to organ development, morphogenesis and physiological traits. *Plant Cell Physiol.* **46**, 48–62.

Liu, J.L. (2010) Intracellular compartmentation of CTP synthase in *Drosophila. J. Genet. Genom.* **37**, 281–296.

Liu, J.L. (2016) The cytoophidium and its kind: filamentation and compartmentation of metabolic enzymes. *Ann. Review Cell Develop. Biol.* **32**, 349–372.

Liu, J.L. and Gall, J.G. (2007) U bodies are cytoplasmic structures that contain uridine-rich small nuclear ribonucleoproteins and associate with P bodies. *Proc. Natl Acad. Sci. USA* **104**, 11655–11659.

Liu, J.L., Murphy, C., Buszczak, M., Clatterbuck, S., Goodman, R. and Gall, J.G. (2006) The Drosophila melanogaster Cajal body. *J. Cell Biol.* **172**, 875–884.

Lo, S.F., Cheng, M.L., Hsing, Y.C., Chen, Y.S., Lee, K.W., Hong, Y.F., Hsiao, Y. *et al.* (2020) Rice Big Grain 1 promotes cell division to enhance organ development, stress tolerance and grain yield. *Plant Biotechnol. J.* **18**, 1969–1983.

Lopes, M.A. and Larkins, B.A. (1993) Endosperm origin, development, and function. *Plant Cell*, **5**, 1383–1399.

Lynch, E.M., Hicks, D.R., Shepherd, M., Endrizzi, J.A., Maker, A., Hansen, J.M., Barry, R.M. *et al.* (2017) Human CTP synthase filament structure reveals the active enzyme conformation. *Nat. Struct. Mol. Biol.* **24**, 507–514.

Lyu, J., Wang, D., Duan, P., Liu, Y., Huang, K.e., Zeng, D., Zhang, L. *et al.* (2020) Control of grain size and weight by the GSK2-LARGE1OML4 pathway in rice. *Plant Cell*, **32**, 1905–1918.

Miao, J., Guo, D., Zhang, J., Huang, Q., Qin, G., Zhang, X., Wan, J. *et al.* (2013) Targeted mutagenesis in rice using CRISPR-Cas system. *Cell Res.* **23**, 1233–1236.

Nagasawa, N., Hibara, K.I., Heppard, E.P., Vander Velden, K.A., Luck, S., Beatty, M., Nagato, Y. *et al.* (2013) *GIANT EMBRYO* encodes CYP78A13, required for proper size balance between embryo and endosperm in rice. *Plant J.* **75**, 592–605.

Noree, C., Monfort, E., Shiau, A.K. and Wilhelm, J.E. (2014) Common regulatory control of CTP synthase enzyme activity and filament formation. *Mol. Biol. Cell* **25**, 2282–2290.

Noree, C., Sato, B.K., Broyer, R.M. and Wilhelm, J.E. (2010) Identification of novel filament-forming proteins in *Saccharomyces cerevisiae* and *Drosophila melanogaster. J. Cell Biol.* **190**, 541–551.

Olsen, O.A. (2004) Nuclear endosperm development in cereals and *Arabidopsis thaliana. Plant Cell*, **16**, S214–S227.

Pasriga, R., Cho, L.H., Yoon, J. and An, G. (2018) Identification of the regulatory region responsible for vascular tissue–specific expression in the rice *Hd3a* promoter. *Mol. Cells*, **41**, 342–350.

Paul, P., Dhatt, B.K., Miller, M., Folsom, J.J., Wang, Z., Krassovskaya, I., Liu, K. *et al.* (2020) *MADS78* and *MADS79* are essential regulators of early seed development in rice. *Plant Physiol.* **182**, 933–948.

Pignocchi, C., Minns, G.E., Nesi, N., Koumproglou, R., Kitsios, G., Benning, C., Lloyd, C.W. *et al.* (2009) ENOSPERM DEFECTIVE1 is a novel microtubule-associated protein essential for seed development in Arabidopsis. *Plant Cell*, **21**, 90–105.

Qi, D., Wen, Q., Meng, Z., Yuan, S., Guo, H., Zhao, H. and Cui, S. (2020) *OsLFR* is essential for earyl endosperm and embryo development by interacting with SWI/SNF complex members in *Oryza sativa. Plant J.* **104**, 901–916.

Sabelli, P.A. and Larkins, B.A. (2009) The Development of endosperm in grasses. *Plant Physiol.* **149**, 14–26.

Shen, Y.-J., Jiang, H., Jin, J.-P., Zhang, Z.-B., Xi, B., He, Y.-Y., Wang, G. *et al.* (2004) Development of genome-wide DNA polymorphism data base for map-based cloning of rice genes. *Plant Physiol.* **35**, 1198–1205.

Sheth, U. and Parker, R. (2006) Targeting of aberrant mRNAs to cytoplasmic processing bodies. *Cell*, **127**, 1095–1109.

Su'udi, M., Cha, J.-Y., Jung, M.H., Ermawati, N., Han, C.-D., Kim, M.G., Woo, Y.-M. *et al.* (2012) Potential role of the rice *OsCCS52A* gene in endoreduplication. *Planta*, **235**, 387–397.

Sun, X., Ling, S., Lu, Z., Ouyang, Y., Liu, S. and Yao, J. (2014) OsNF-YB1, a rice endosperm-specific gene, is essential for cell proliferation in endosperm development. *Gene*, **551**, 214–221.

Xing, Y. and Zhang, Q. (2010) Genetic and molecular bases of rice yield. *Annu. Rev. Plant Biol.* **61**, 421–442.

Yang, B., Wendrich, J.R., Rybel, B.D., Weijers, D. and Xue, H.W. (2020) Rice microtubule-associated protein IQ67-DOMAIN14 regulates grain shape by modulating microtubule cytoskeleton dynamics. *Plant Biotechnol. J.* **18**, 1141–1152.

Yang, W., Gao, M., Yin, X., Liu, J., Xu, Y., Zeng, L., Li, Q. *et al.* (2013) Control of rice embryo development, shoot apical meristem maintenance, and grain yield by a novel cytochrome P450. *Mol. Plant* **6**, 1945–1960.

Yi, J. and An, G. (2013) Utilization of T-DNA tagging lines in rice. *J. Plant Biol.* **56**, 85–90.

Yoon, J., Cho, L.H., Kim, S.L., Choi, H., Koh, H.J. and An, G. (2014) The BEL1-type homeobox gene *SH5* induces seed shattering by enhancing abscission-zone development and inhibiting lignin biosynthesis. *Plant J.* **79**, 717–728.

Yoon, J., Cho, L.H., Antt, H.W., Koh, H.J. and An, G. (2017) KNOX protein OSH15 induces grain shattering by repressing lignin biosynthesis genes. *Plant Physiol.* **174**, 312–325.

Yoon, J., Cho, L.H., Lee, S., Pasriga, R., Tun, W., Yang, J., Yoon, H. *et al.* (2019) Chromatin interacting factor OsVIL2 is required for outgrowth of axillary buds in rice. *Mol. Cells* **42**, 858–868.

Yoon, J., Cho, L.H., Yang, W., Pasriga, R., Wu, Y., Hong, W.J., Bureau, C. *et al.* (2020) Homeobox transcription factor OsZHD2 promotes root meristem activity in rice by inducing ethylene biosynthesis. *J. Exp. Bot.* **71**, 5348–5364.

Zhou, S.R., Yin, L.L. and Xue, H.W. (2013) Functional genomics based understanding of rice endosperm development. *Curr. Opin. Plant Biol.* **16**, 236–246.

Supporting information

Additional supporting information may be found online in the Supporting Information section at the end of the article.

Figure S1 Phylogenetic tree of CTPS genes from 44 plant species.
Figure S2 Phylogenetic tree of CTPS genes from five plant species: Arabidopsis, rice, maize, *Sorghum bicolor*, and *Glycine max*.
Figure S3 Digital expression patterns of six CTPS genes in rice.
Figure S4 Generation of *osctps1* null mutants using CRISPR/Cas9.
Figure S5 Phenotypes of WT and *enl2-2* mutants.
Figure S6 Phenotypes of WT and *enl2-2* mutant at seedling stages.
Figure S7 Seed phenotypes of WT and *enl2-2* mutants.
Figure S8 Embryo development of WT and *enl2-2*.
Figure S9 Expression levels of genes involved in cell cycle and mitosis in WT and *enl2-2* at 3 HAP and 24 HAP.
Figure S10 Characterization of *OsCTPS1*-overexpressing plants.
Table S1 Primers used for fine mapping and sequencing of Os01g43020.
Table S2 List of primers used in this study.